Supporting Information for

Mechanistic Studies of Bioorthogonal ATP Analogues for Assessment of Histidine Kinase Autophosphorylation

Adeline Espinasse,[a] Xuelan Wen,[a] Jason D. Goodpaster[a] and Erin E. Carlson*[,a,b,c]

[a]*Department of Chemistry, University of Minnesota, 207 Pleasant Street SE, Minneapolis, Minnesota 55455, United States*
[b]*Department of Medicinal Chemistry, University of Minnesota, 208 Harvard Street SE, Minneapolis, Minnesota 55454, United States*
[c]*Department of Biochemistry, Molecular Biology, and Biophysics, University of Minnesota, 321 Church St SE, Minneapolis, Minnesota 55454, United States*
**Corresponding Author*

GENERAL INFORMATION AND METHODS.

Materials. ATPγNH-propargyl (cat # 808512) was purchased from Sigma-Aldrich, ATP-propargyl (cat # CLK-T10-1) from Jena Bioscience, TAMRA-PEG3-N_3 (cat# BP22479) from BroadPharm and BODIPY-FL-ATPγS (cat# A22184) from ThermoFisher. [γ-33P]-ATP was purchased from Hartmann Analytic (cat# SCF-301). All other reagents were purchased from commercial sources, unless otherwise indicated, and used as without further purification and as directed.

HK853 Protein expression and purification. Total gene synthesis of HK853, protein production and expression were performed according to Wilke et al. and Chase et al. In summary, the gene corresponding to the cytoplasmic portion of HK853 from *T. maritima* was ligated into the pHis-parallel 1 vector with a His-tag at the N-terminus. The recombinant plasmids were transformed into *E. coli* DH5α then in *E. coli* BL21(DE3)Rosetta/pLysS overexpression cells and plated on LB agar containing 34 μg/mL chloramphenicol and 100 μg/mL ampicillin. Plates were incubated at 37 °C overnight. A single colony was transferred to 10 mL of LB media supplemented with antibiotics as noted above. The cells were grown at 37 °C at 220 RPM overnight. To 1 L of LB media containing the antibiotics noted above, 10 mL of the previous culture were added. The cells were grown at 37 °C and 220 RPM until the OD_{600} of the solution was about 0.6. The culture was allowed to cool to room temperature. The cultures were induced with 220 µL of 1 M IPTG and incubated at 20 °C and 220 RPM for 20 h. Subsequently, the cells were spun down at 8,000 x *g* for 40 min. The supernatant was discarded. The pellets were kept in the storage buffer (10 mM Tris, 0.1 mM EDTA, 0.5 M NaCl, 12% glycerol, 2 mM DTT, pH = 7.6) at -80 °C. Then, the lysis buffer (50 mL, Tris 25mM, NaCl 1 M, glycerol 10%, imidazole 5 mM, DTT 2 mM, pH = 8), 1 tablet of mini EDTA free Roche and DNAse (10 µg/1 L) were added. The suspension was homogenized with a hand glass homogenizer (10 times). The cells were lysed by sonication on ice (2 min sonication, every 5 minutes for 30 min, power 3) and spun down. The supernatant was passed through on a 0.22 µm filter. The solution was frozen on dry ice and kept at -80 °C until purification. The protein was purified via nickel affinity column (Ni-NTA) on GE ÄKTAFPLC using buffer A (Tris 25 mM, NaCl 1 M, glycerol 10%, imidazole 5 mM, DTT 2 mM, pH = 8) and buffer B (Tris 25 mM, NaCl 1 M, glycerol 10%, imidazole 1 M, DTT 2 mM, pH= 8) with a gradient of 5 mM to 1 M of imidazole. The detection was done at 210 nm. HK853 was further purified via size exclusion using HiLoad 16/60 Superdex 200 pg column using a storage buffer (10 mM Tris, 0.1 mM EDTA, 0.5 M NaCl, 12% glycerol, 2 mM DTT, pH = 7.6) as the eluent.[1]

Protein concentration determination. Protein concentration was determined using an Implen's Nanophotometer spectrophotometer (Thermo Fisher Scientific) at 280 nm.

Reaction buffer. The reaction buffer was composed of 50 mM Tris-HCl, pH 7.8, 200 mM KCl, 5 mM $MgCl_2$.

SDS-PAGE (Sodium dodecyl sulfate-polyacrylamide gel electrophoresis) gel. A 12% separating gel was prepared using MilliQ water (21 mL), 40% acrylamide/bisacrylamide

(10.5 mL) 1.5 M Tris.HCl, pH = 8.8 (10.5 mL), 10% ammonium persulfate (140 µL), TEMED (15 µL). The stacking gel was added to the cassette and 250 µL of ethanol was added to allow for polymerization (1 h). The ethanol was removed, and the gel was washed with MilliQ water. The 4.5% stacking gel was prepared with MilliQ water (6.4 mL), 40% acrylamide/bisacrylamide (29:1, 1.125 mL) 0.5 M Tris.HCl, pH = 6.8 (2.5 mL),10% ammonium persulfate (30 µL), TEMED (10 µL). Running parameters were 180 V, 400 mA, and 60 W for 1 h. SDS-PAGE running buffer was diluted ten-fold from a 10X Tris-Glycine SDS Running buffer and chilled during electrophoresis.

SDS-PAGE loading buffer. 4X SDS-PAGE sample loading buffer containing 200 mM Tris, pH 6.8, 40% glycerol, 8% SDS (w/v), 4% β-mercaptoethanol, and 0.8% bromophenol blue (w/v) was used.

In-gel fluorescence detection. After SDS-PAGE, the gels were washed 3 times with MilliQ water and scanned using a Typhoon FLA 9500 scanner (GE Healthcare) at 532 nm (long-pass filter) detection for TAMRA (λex: 542 nm, λem: 568 nm) and 526-nm (short-pass filter) detection for BODIPY-FL (λex: 504 nm, λem: 514 nm). Integrated density measurements were determined using ImageJ. Any changes in brightness or contrast were performed uniformly over the entire gel.

Protein loading determination in SDS-PAGE gel. After fluorescent scanning, the gels were microwaved for 30 s in Coomassie Brilliant Blue R-250 Staining Solution (cat# 1610436) and incubated in this solution for 15 min. The gels were destained overnight using a 10% acetic acid solution and scanned using the Typhoon instrument (setting: excitation 532 nm, emission filter 570 BP 20).

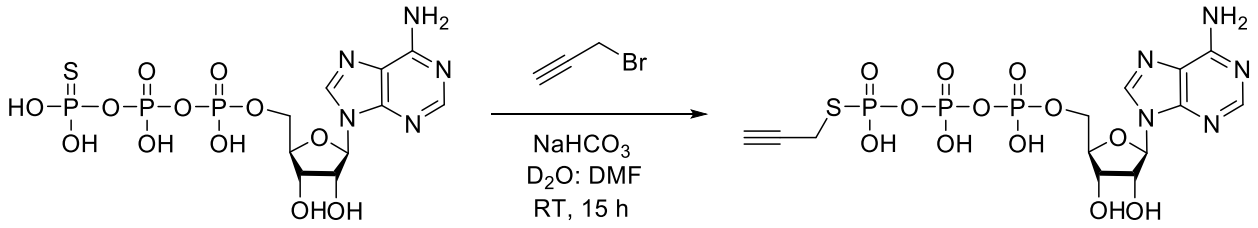

Supplementary Scheme 1. Reaction scheme for the synthesis of Probe O.

ATPγS lithium salt (2 mg, 3.7 µmol) was dissolved in D_2O (3 mL) and DMF (50 µL). Sodium bicarbonate (0.3 mg, 3.7 µmol) was added followed by propargyl bromide (0.5 µL, 5.6 µmol). The reaction was stirred at room temperature for 15 h. After determination of completion by ^{31}P NMR, the product was purified by RP-HPLC using an Agilent 1200 series equipped with Agilent Zorbax C3, 5 µm, 9.4 x 250 mm and a gradient of 0.1 % ammonium acetate in water (Buffer A) and 0.1% ammonium acetate in acetonitrile (Buffer B); 0-3 min 95% Buffer A; 3-10 min 95 to 5% Buffer A; 10-12 min 5% Buffer A. The collected fractions were lyophilized several times to afford the product as a white solid. Yield = 52%, white solid as the ammonium salt. ^1H NMR (D_2O, 500 MHz) δ 8.538 (s, 1H, C1**H**), 8.263 (s, 1H, C7**H**), 6.148 (d, J = 6.5 Hz, 1H, C11**H**), 4.790 (m, 1H, C15**H**), 4.586 (t, J = 4.5 Hz, 1H, C14**H**), 4.407 (quint, 1H, C13**H**) 4.272 (m, 2H, C18**H**), 3.568 (d, J =

12.5 Hz, 1H, C**H₂**CCH), 2.503 (t, J = 3 Hz, 1H, CH_2CC**H**); ^{13}C NMR (D_2O, 500 MHz) δ 155.68, 152.85, 149.03, 139.84, 118.70, 86.71, 84.01, 83.94, 74.28, 71.78, 70.36, 65.28, 17.91 ^{31}P NMR (D_2O, 400 MHz) 6.52 (d, 1P, $J_{P\beta,P\gamma}$ = 66 Hz, γ), -11.60 (d, 1P, $J_{P\alpha,P\beta}$ = 48 Hz, α), -24.04 (dd, 1P, $J_{P\beta,P\gamma}$ = 66 Hz, $J_{P\alpha,P\beta}$ = 48 Hz, β). δ ESI-MS (negative): [M-H] = 559.9813 (calcd.), 559.9844 (found).

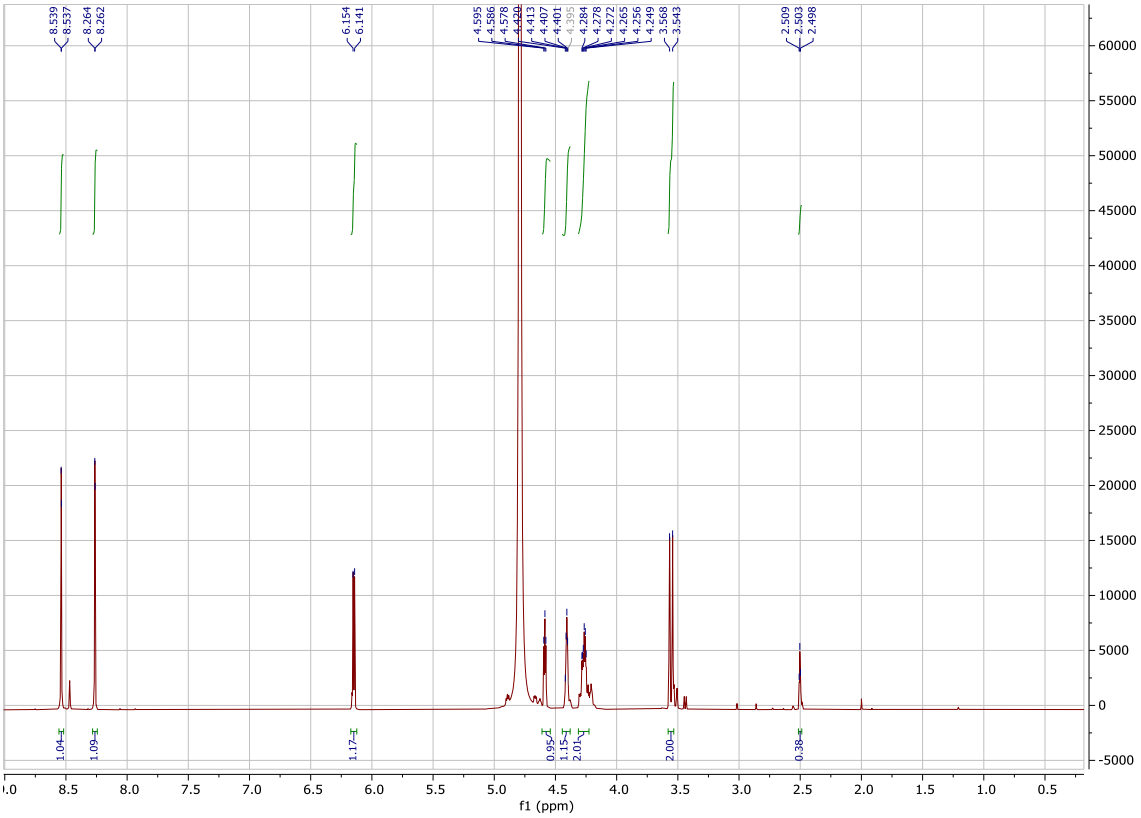

^1H NMR spectrum of Probe S.

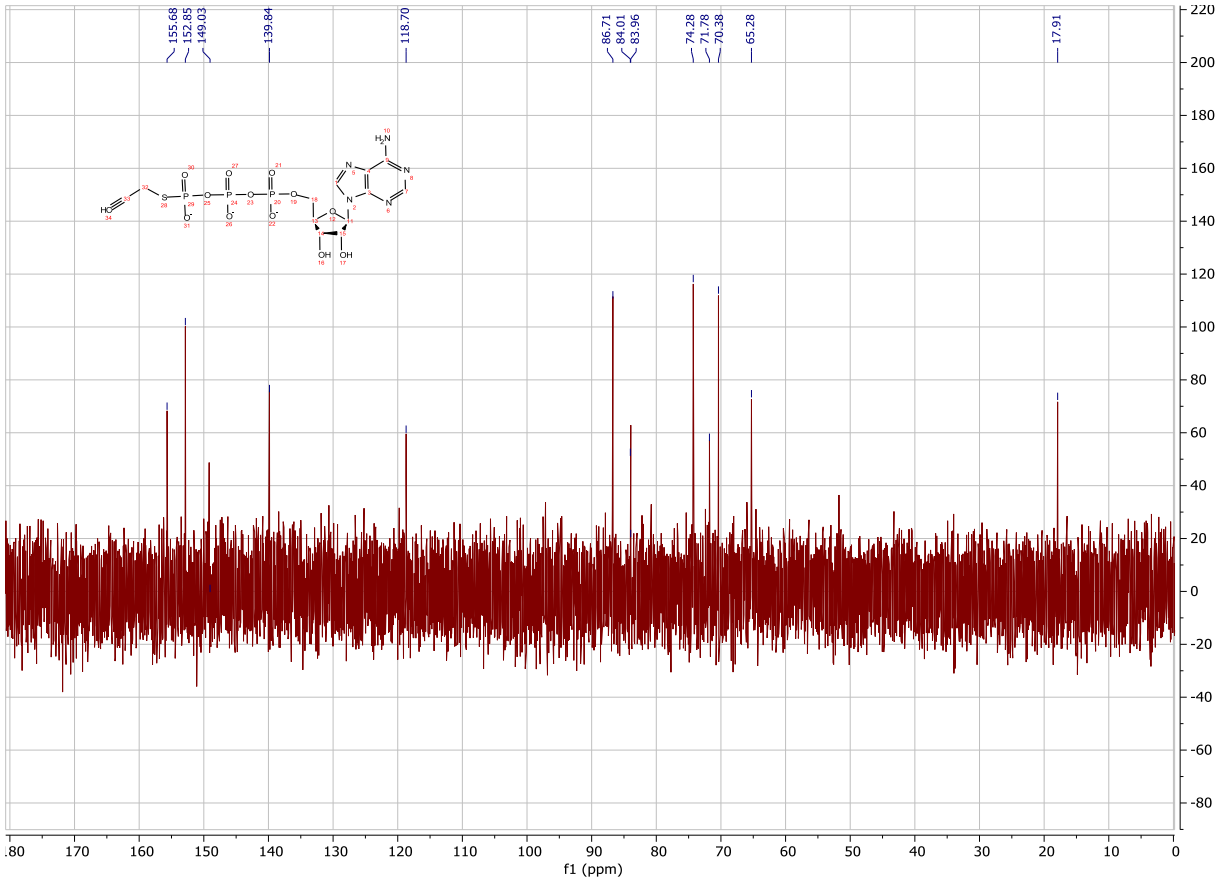

^{13}C NMR spectrum of Probe S.

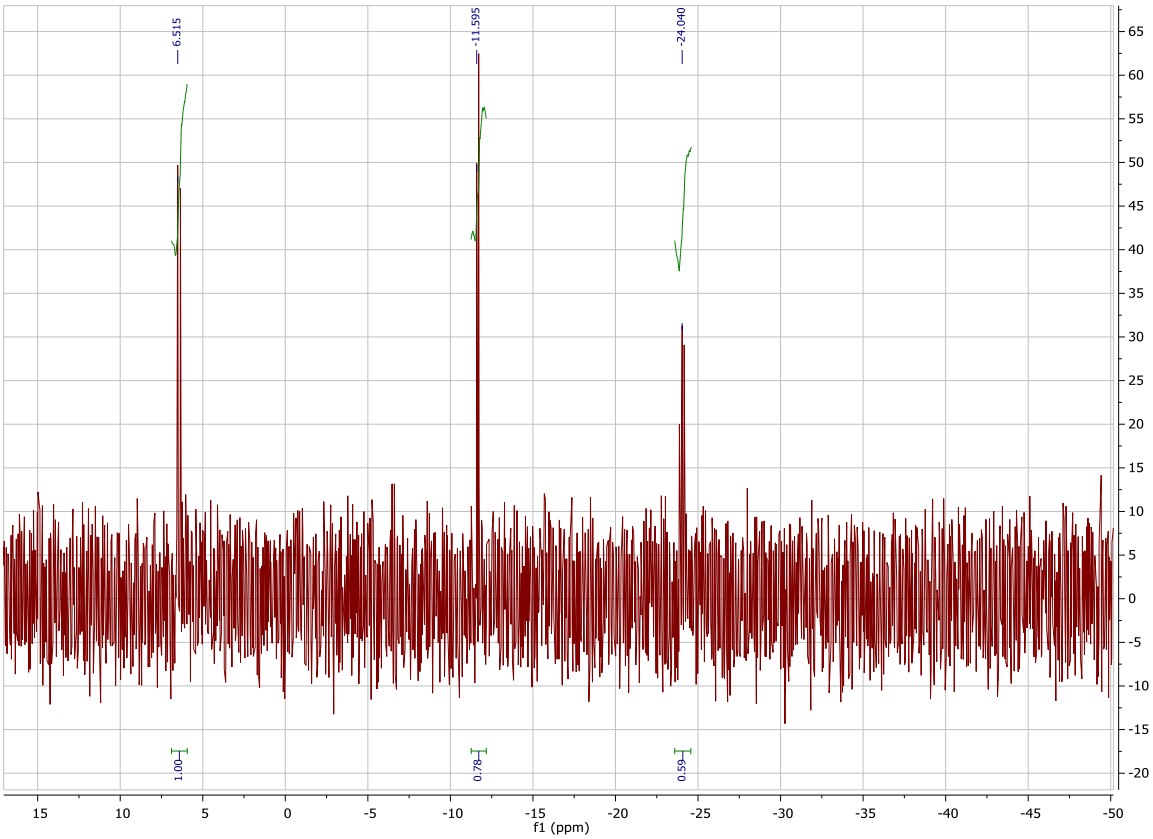

^{31}P NMR spectrum of Probe S.

Assays

The intensities resulting from TAMRA and BODIPY-FL fluorescence and Coomassie were measured using ImageJ software. Background and blanks were subtracted from all the bands.

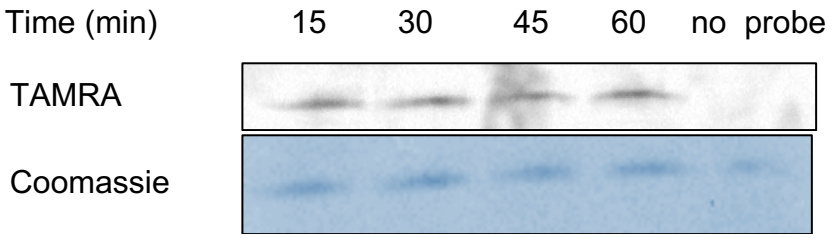

Incubation time (min)	Integrated density (A. U.)
15	12.4
30	10.5
45	11.0
60	11.3

Supplementary Figure 1. Time dependent CuAAC labeling of HK853 with Probe O. HK853 (1 μM) was incubated with Probe O (45 μM) in 25 μL. Samples were quenched with PBS containing 10% SDS and 10% triton X-100 (2.5 μL) at 15 min. The solutions were "clicked" with TAMRA-N_3 (1 μL of 5 mM stock solution), TCEP (0.8 μL of 50 mM stock solution), TBTA (0.4 μL of 10 mM stock solution) and $CuSO_4$ (0.8 μL of 50 mM stock solution) for various times. Samples were run on 12 % SDS-PAGE gel and scanned. The resulting labeling of HK853 shows similar intensity between 15 min and 1 h incubation of the CuAAC reagents with phosphorylated protein. Thus, we decided to run the CuAAC for 30 min.[2]

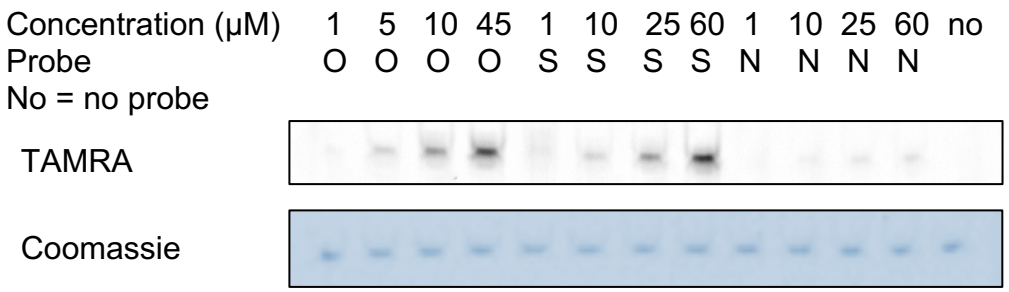

Supplementary Figure 2. Concentration dependent assay comparison of HK autophosphorylation with Probe O, S and N (range from 1 to 60 μM). HK853 (1 μM) was incubated with Probes S, O, N (range from 1 to 60 μM) in 25 μL of reaction buffer for 15 min. The reactions were quenched with PBS containing 10% SDS 10% triton X-100 (2.5 μL). The solutions were "clicked" with TAMRA-N_3 (1 μL of 5 mM stock solution), TCEP (0.8 μL of 50 mM stock solution), TBTA (0.4 μL of 10 mM stock solution) and $CuSO_4$ (0.8 μL of 50 mM stock solution) for 30 min. The samples were run on a 12 % SDS-PAGE gel and scanned.

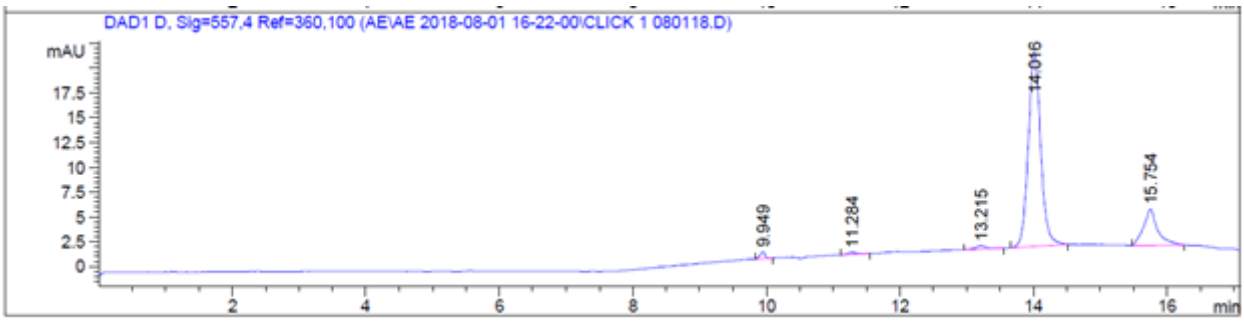

Supplementary Figure 3. HPLC chromatogram of the formation of the TAMRA-triazole-aminophosphate as a mimic of phosphorylated HK853. Propargyl-aminophosphate (50 μM) was incubated in PBS with 1% in SDS (100 μL) with TAMRA-N_3 (125 μM), TCEP (1 mM), TBTA (0.1 mM) and $CuSO_4$ (1 mM) for 30 min. The reaction was quench by the introduction of the sample in the HPLC. The reaction was followed at 557 nm, the absorbance wavelength of TAMRA. Peak at 14.016 min (area under the curve 88.00491 mAU.s): excess TAMRA- N_3, peak at 15.754 (area under the curve 19.38400 mAU.s): TAMRA-triazole-aminophosphate. Based on the amounts of propargyl-aminophosphate introduced, of TAMRA- N_3 and the amount of product formed, the yield is 45%.

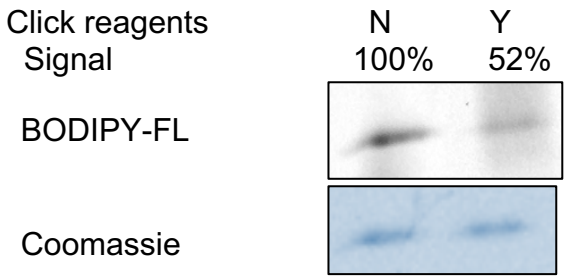

Supplementary Figure 4. Impact of the CuAAC reagents on HK853 labeling by B-FL-ATPγS. HK853 (1 μM) was incubated with B-FL-ATPγS (60 μM) in 25 μL of reaction buffer for 15 min. The reactions were quenched with PBS with 10% SDS and 10% triton X-100 (2.5 μL). To the reactions, either the loading buffer (18 μL) was added or the click reagents TAMRA-N_3 (1 μL of 5 mM stock solution), TCEP (0.8 μL of 50 mM stock solution), TBTA (0.4 μL of 10 mM stock solution) and $CuSO_4$ (0.8 μL of 50 mM stock solution) for 1 h followed by the loading buffer (15 μL) to mimic the effects of the CuAAC conditions on the phosphohistidine formation. The samples were run on a 12 % SDS-PAGE gel and scanned. The background was subtracted to each intensity value. The values were adjusted based on the Coomassie intensity of each band before calculating the percent labeling. (n = 3).

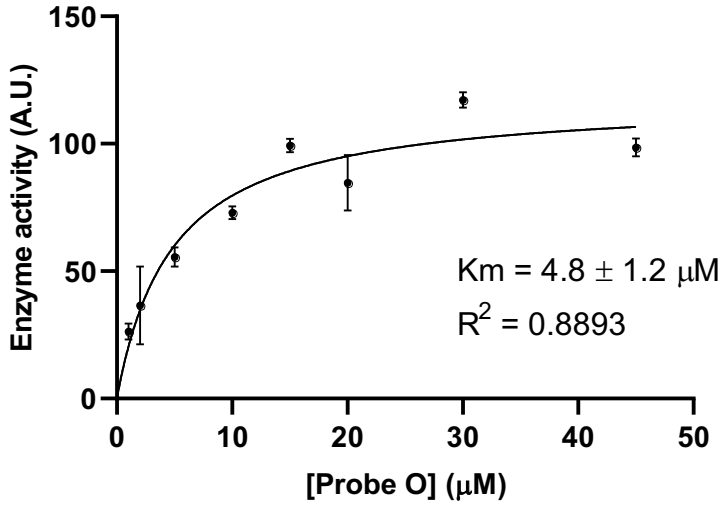

Concentration (μM) 1 2 5 10 15 20 30 45 no
No = no probe

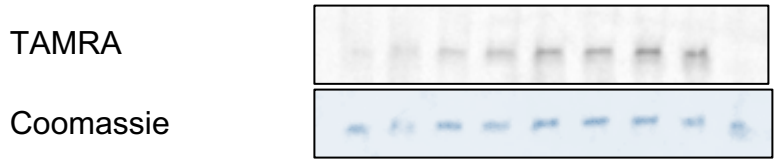

Supplementary Figure 5. Concentration dependent assay of HK autophosphorylation with Probe O. HK853 (1 μM) was incubated with various concentration of Probe O (1–45 μM) in 25 μL. Samples (25 μL) were quenched with PBS containing 10% SDS and 10% triton X-100 (2.5 uL) at 15 min. The solutions were "clicked" with TAMRA-N_3 (1 μL of 5 mM stock solution), TCEP (0.8 μL of 50 mM stock solution), TBTA (0.4 μL of 10 mM stock solution) and $CuSO_4$ (0.8 μL of 50 mM stock solution) for 30 min. The samples were run on 12% SDS-PAGE gel and scanned (n = 2).[3-4]

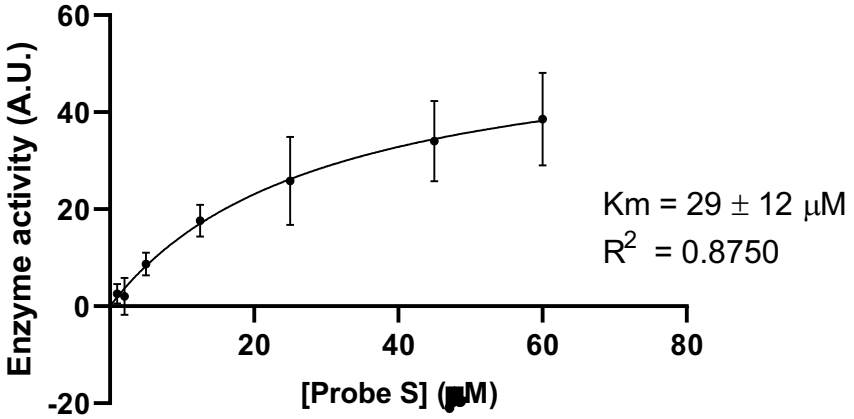

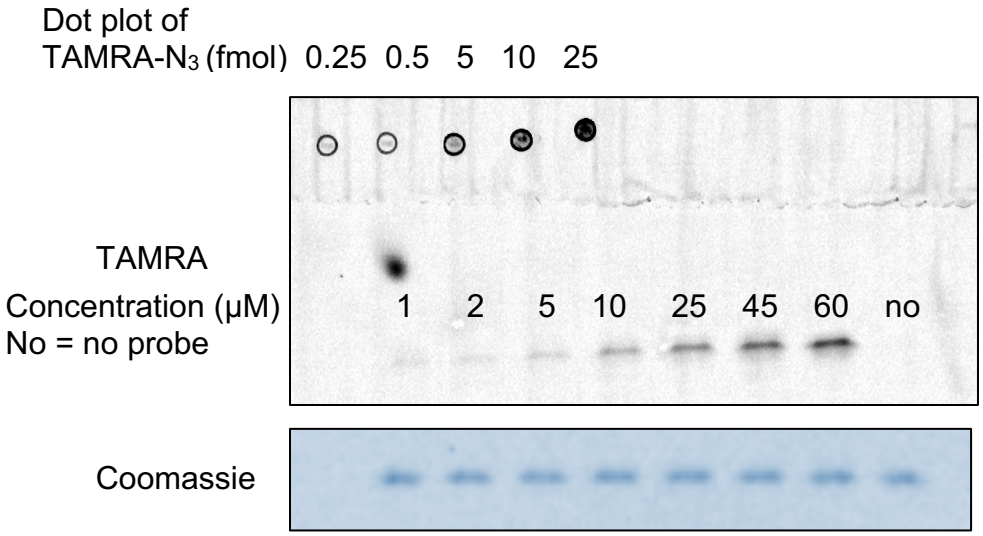

Supplementary Figure 6. Concentration dependent assay of HK autophosphorylation with Probe S. HK853 (1 μM) was incubated with various concentration of Probe S (1–60 μM) in 25 μL. Samples (25 μL) were quenched with PBS containing 10% SDS and 10% triton X-100 (2.5 μL) at 15 min. The solutions were "clicked" with TAMRA-N_3 (1 μL of 5 mM stock solution), TCEP (0.8 μL of 50 mM stock solution), TBTA (0.4 μL of 10 mM stock solution) and $CuSO_4$ (0.8 μL of 50 mM stock solution) for 60 min. The samples were run on 12% SDS-PAGE gel and scanned (n = 3). For this assay, the gels were run separately and a dot plot with known amounts of TAMRA-N_3 was used to quantify the band intensities (1 μL of 0.25 nM, 0.5 nM, 5 nM, 10 nM, 25 nM).[3-4]

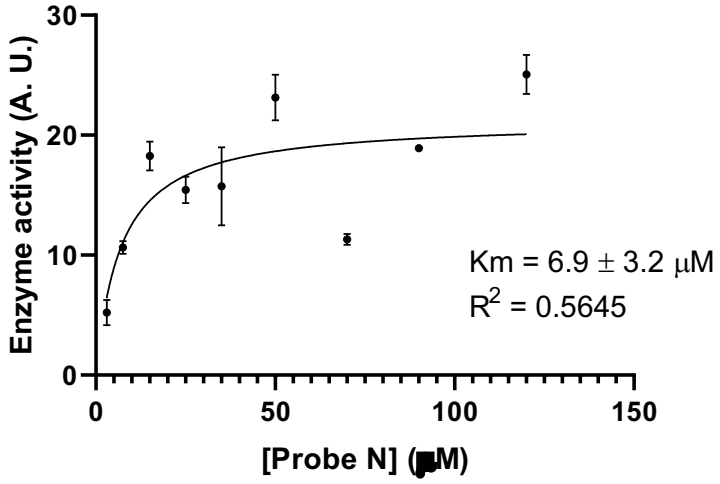

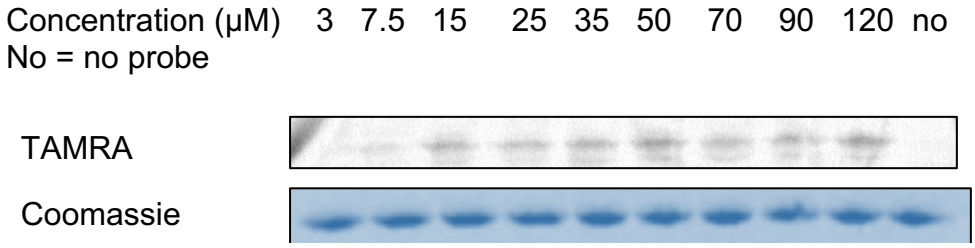

Supplementary Figure 7. Concentration dependent assay of HK autophosphorylation with Probe N. HK853 (3 μM) was incubated with various concentration of Probe N (1–120 μM) in 25 μL. Samples (25 μL) were quenched with PBS containing 10% SDS and 10% triton X-100 (2.5 μL) at 15 min. The solutions were "clicked" with TAMRA-N_3 (1 μL of 5 mM stock solution), TCEP (0.8 μL of 50 mM stock solution), TBTA (0.4 μL of 10 mM stock solution) and $CuSO_4$ (0.8 μL of 50 mM stock solution) for 30 min. The samples were run on 12% SDS-PAGE gel and scanned (n = 2).[3-4]

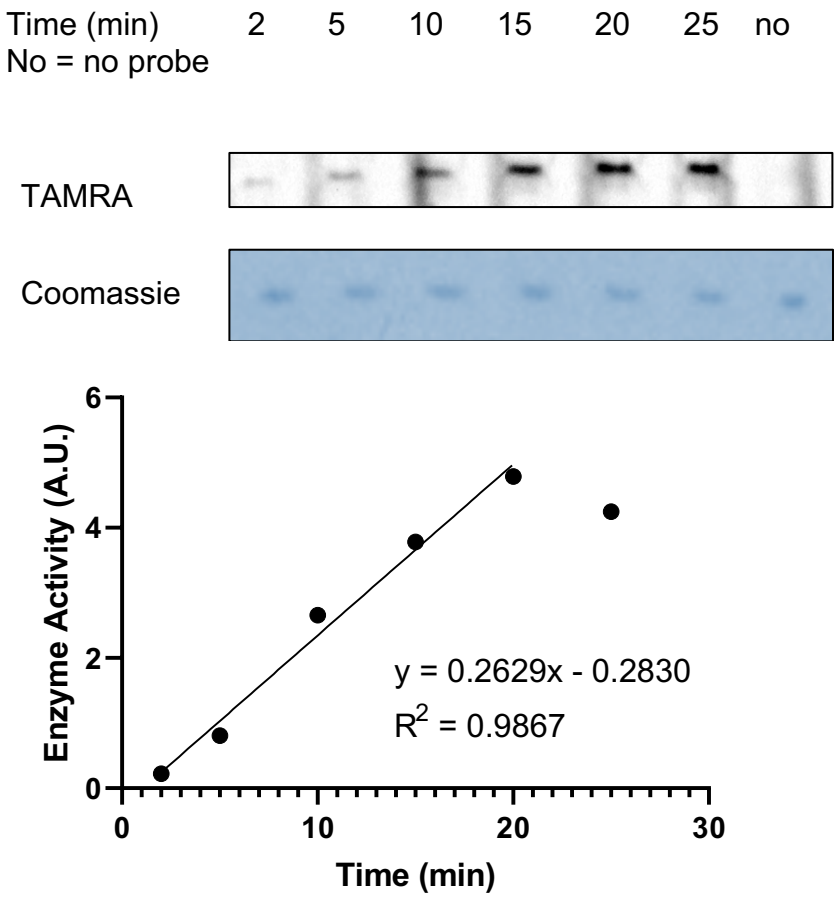

Supplementary Figure 8. Time dependent labeling of HK853 with Probe O. HK853 (1 μM) was incubated with Probe O (45 μM) in 200 μL. Samples (25 μL) were taken at 2, 5, 10, 15, 20 and 30 min and quenched with PBS containing 10% SDS and 10% triton X-100 (2.5 μL). The solutions were "clicked" with TAMRA-N_3 (1 μL of 5 mM stock solution), TCEP (0.8 μL of 50 mM stock solution), TBTA (0.4 μL of 10 mM stock solution) and $CuSO_4$ (0.8 μL of 50 mM stock solution) for 30 min. The samples were run on 12% SDS-PAGE gel and scanned.[3-4]

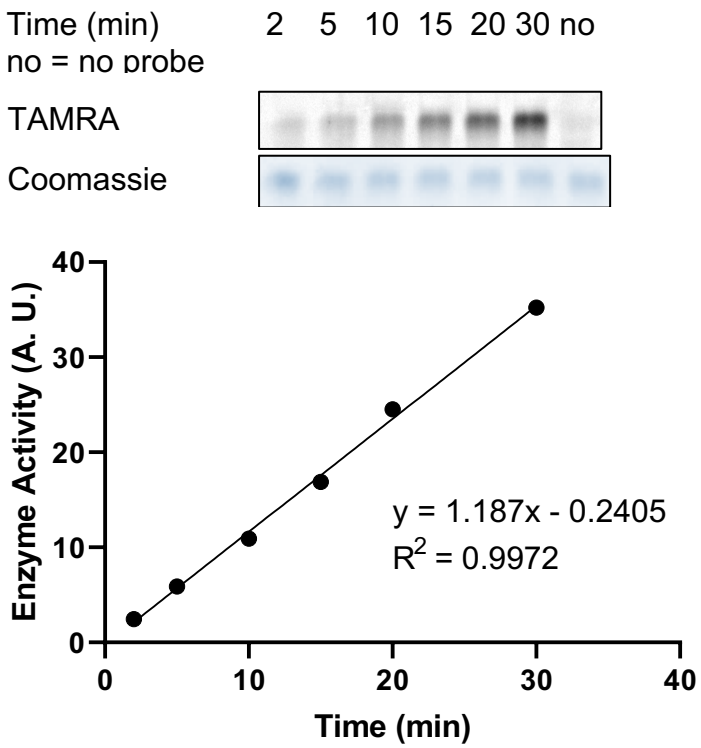

Supplementary Figure 9. Time dependent labeling of HK853 with Probe S. HK853 (1 μM) was incubated with Probe S (60 μM) in 200 μL. Samples (25 μL) were taken at 2, 5, 10, 15, 20 and 30 min and quenched with PBS containing 10% SDS and 10% triton X-100 (2.5 μL). The solutions were "clicked" with TAMRA-N_3 (1 μL of 5 mM stock solution), sodium ascorbate (2 μL of 100 mM stock solution), THPTA (0. μL of 50 mM stock solution) and $CuSO_4$ (0.2 μL of 20 mM stock solution) for 60 min. The samples were run on 12% SDS-PAGE gel and scanned.[3-4]

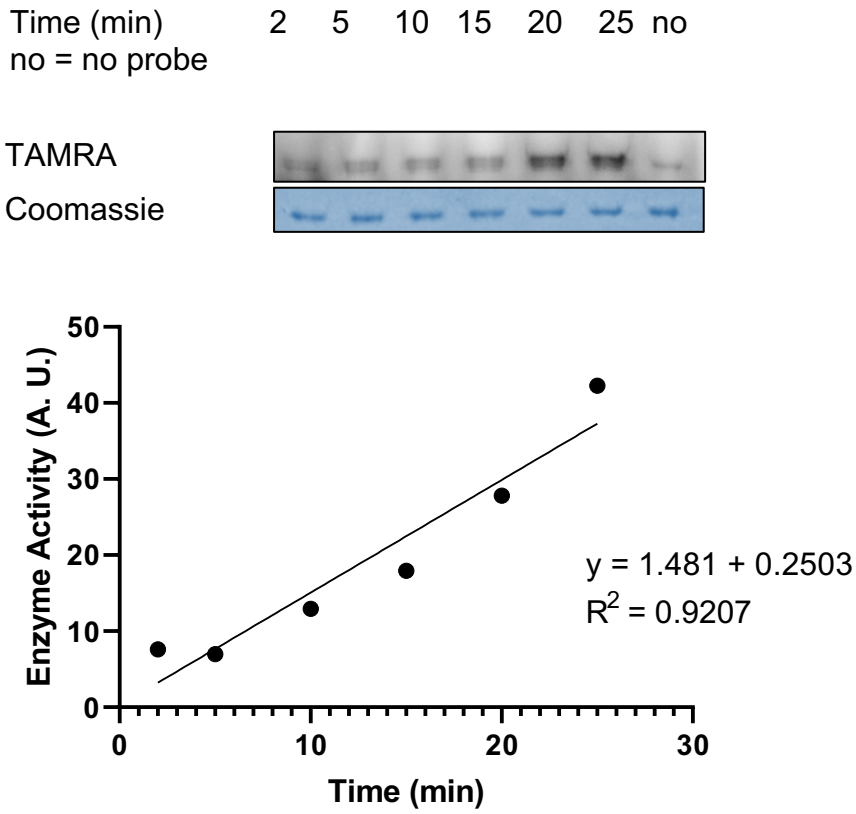

Supplementary Figure 10. Time dependent labeling of HK853 with Probe N. HK853 (3 μM) was incubated with Probe N (120 μM) in 200 μL. Samples (25 μL) were taken at 2, 5, 10, 15, 20 and 30 min and quenched with PBS containing 10% SDS and 10% triton X-100 (2.5 μL). The solutions were "clicked" with TAMRA-N_3 (1 μL of 5 mM stock solution), TCEP (0.8 μL of 50 mM stock solution), TBTA (0.4 μL of 10 mM stock solution) and $CuSO_4$ (0.8 μL of 50 mM stock solution) for 30 min. The samples were run on 12% SDS-PAGE gel and scanned.[3-4]

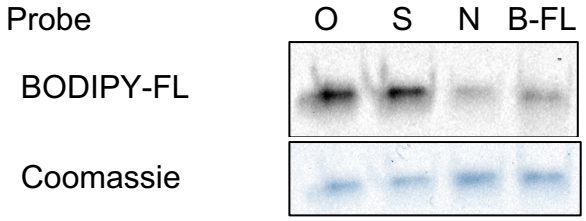

Supplementary Figure 11. Labeling comparison between Probe S, O, N and B-FL-ATPγS. HK853 (2 μM) was incubated with Probe S, O, N and B-FL-ATPγS (60 μM in 25 μL) for 15 min. The reactions were quenched with PBS with 10% SDS 10% triton X-100 (2.5 μL). The solutions were "clicked" with B-FL-N_3 (1 μL of 5 mM stock solution), TCEP (0.8 μL of 50 mM stock solution), TBTA (0.4 μL of 10 mM stock solution) and $CuSO_4$ (0.8 μL of 50 mM stock solution) for 30 min. The proteins were precipitated using ProteoExtract® Protein Precipitation Kit using the precipitant agent (150 μL) for 30 min at -20 °C. The solutions were centrifuged at 14000 RPM for 10 min. The supernatant was removed. The proteins were washed with the wash solution (150 μL). PBS with 1% SDS (20 μL) was added to resuspend the proteins and 4X loading buffer was added. The samples were run on 12% SDS-PAGE gel and scanned.

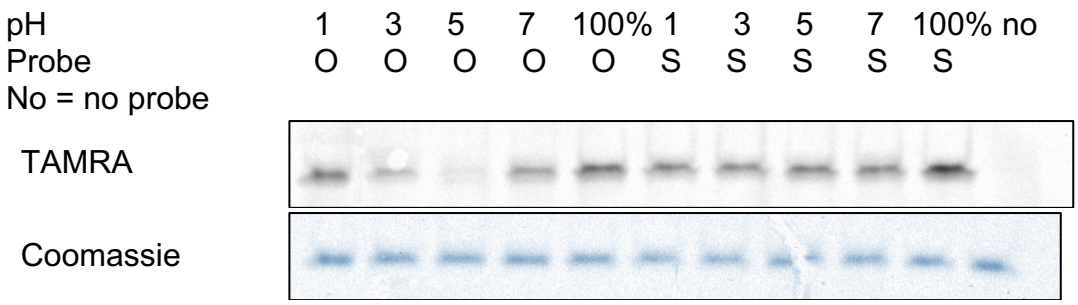

Supplementary Figure 12. Degradation assays at different pH values of the phosphohistidine derivatives from Probes O and S. HK853 (2 μM) was incubated with probe O or S (60 uM in 25 μL) for 15 min. The reactions were quenched with a solution of ADP in PBS (9 mM, 3.5 μL). A solution of 1 M HCl (2, 0.5 or 0.4 μL) was added to reach the desired pH (1, 3 or 5). The reactions were incubated for 3 h, then neutralized. The volumes of the reaction mixtures were normalized by adding water. PBS with 10 % SDS 10% triton (3 μL) was added. The solutions were "clicked" with TAMRA-N_3 (1 μL of 5 mM stock solution), TCEP (0.8 μL of 50 mM stock solution), TBTA (0.4 μL of 10 mM stock solution) and $CuSO_4$ (0.8 μL of 50 mM stock solution) for 30 min. The samples were run on 12% SDS-PAGE gel and scanned. The results were compared to an untreated sample (100%) and normalized to Coomassie staining.

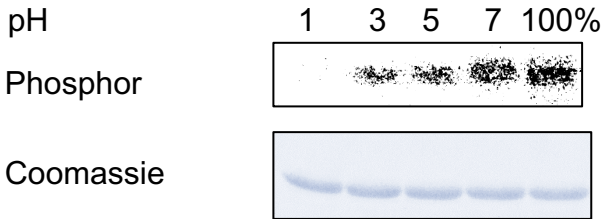

Supplementary Figure 13. Degradation assays at different pH values of the native phosphohistidine. HK853 (2 μM) was incubated with [γ-33P]-ATP (60 μM in 25 μL) for 30 s. The reactions were quenched with a solution of ADP in PBS (9 mM, 3.5 μL). A solution of 1 M HCl (2.0, 0.5 or 0.4 μL) was added to reach the desired pH (1, 3 or 5). The reactions were incubated for 3 h, then neutralized. The volumes of the reaction mixtures were normalized by adding water. The samples were run on 12% SDS-PAGE gel. The gel was fixed for 20 min and dried under vacuum for 2 h at 60 ºC and exposed to a storage phosphor screen for 16 h. The phosphor screen is then scanned. The results were compared to an untreated sample (no 3 h incubation period and pH = 7, 100%) and normalized to Coomassie staining.

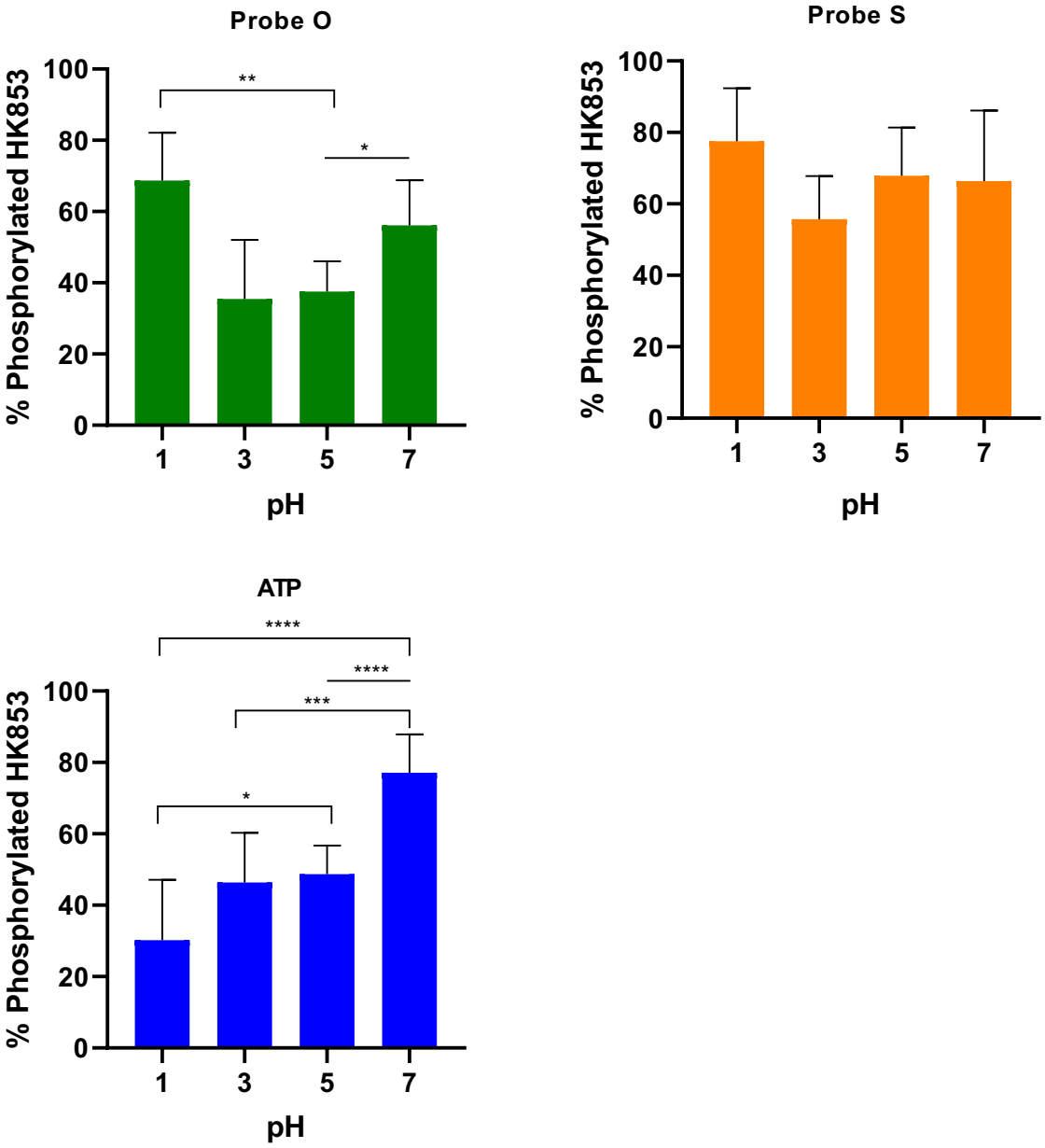

Supplementary Figure 14. Statistical analysis of the hydrolysis studies for each phosphorylated HK853 species between pH values. Statistical analysis to compare two substrates at a specific pH performed with unpaired t-test (****$p \leq 0.0001$; ***$p \leq 0.001$; **$p \leq 0.01$, *$p \leq 0.05$).

Computational methods.

Geometry optimizations were performed using Gaussian 16 program.[5] All geometry optimizations and frequency calculations were performed using the B3LYP functional, the 6-31+G(d) basis set, Grimme's D3 dispersion correction, and the SMD solvation model with water as the solvent. All geometries were characterized by frequency analysis calculations to be local minima (without any imaginary frequency) or transition states (with only one imaginary frequency). All vibrational frequencies below 50 cm^{-1} were replaced with values of 50 cm^{-1} due to the breakdown of the harmonic oscillator model for low frequency vibrational modes. Zero-point vibrational energies and thermal contributions to electronic energy were calculated at 298.15 K and 1 atm. To obtain better estimation of Gibbs free energies, single point electronic energies were computed using B3LYP-D3/6-311+G(d,p) and ωB97XD/6-311+G(d,p) based on the B3LYP-D3/6-31+G(d) geometries.[6] The resulting electronic energies were summed with the thermal free energy contributions computed at the B3LYP-D3/6-31+G(d) level.

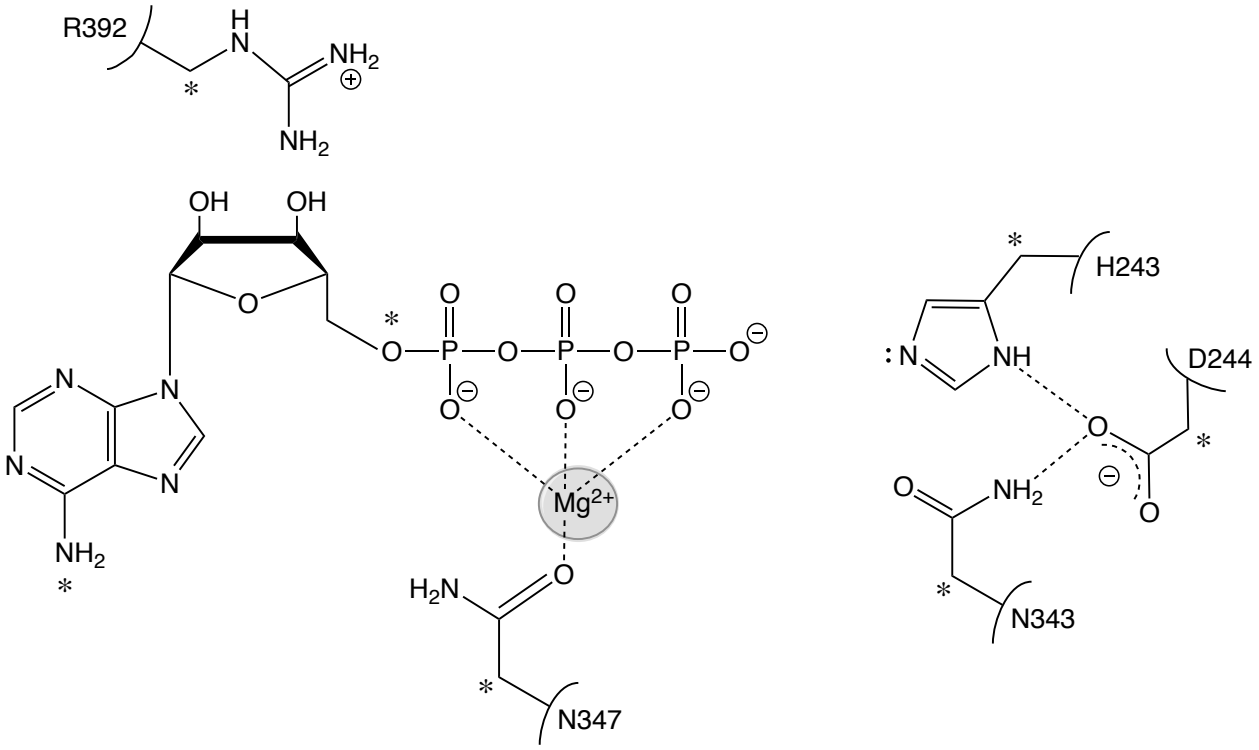

Supplementary Figure 15. Computational model used for HK853 autophosphorylation. The initial geometry was taken from the crystal structure (PDB: 4KP4) and the non-hydrolyzable ATP analogues AMP-PNP was replaced by ATP. Seven atoms (with asterisk) were frozen during the geometry optimizations and frequency calculations. The frozen carbon atoms on amino acid residues were also truncated and then capped with hydrogens. The reactant, transition state, and product of HK853 autophosphorylation are labeled as IM1 (intermediate 1), TS1 (transition state 2), and IM2, respectively.

Supplementary Table 1. Reaction barriers of HK853 autophosphorylation from DFT study for ATP, Probes O, S and N at different level of theories. Reaction barriers $\Delta G^{\ddagger}$(TS1) are given in kcal.mol^{-1}. The SMD model of solvation were included in all calculations.

Probes	Single-point electronic energy		
	B3LYP-D3/6-31+G(d)	B3LYP-D3/6-311+G(d,p)	ωB97XD/6-311+G(d,p)
ATP	12.5	11.6	14.7
Probe O	17.6	16.9	17.7
Probe S	15.2	13.5	14.0
Probe N	20.7	19.3	20.8

Supplementary Table 2. Reaction thermodynamics of HK853 autophosphorylation from DFT study for Probes O, S and N at different level of theories. Reaction thermodynamics ΔG(IM2) are given in kcal.mol^{-1}. The SMD model of solvation were included in all calculations.

Probes	Single-point electronic energy method		
	B3LYP-D3/6-31+G(d)	B3LYP-D3/6-311+G(d,p)	ωB97XD/6-311+G(d,p)
ATP	-8.1	-9.4	-8.2
Probe O	-6.7	-6.4	-5.8
Probe S	-6.8	-7.5	-7.8
Probe N	-7.5	-9.3	-8.7

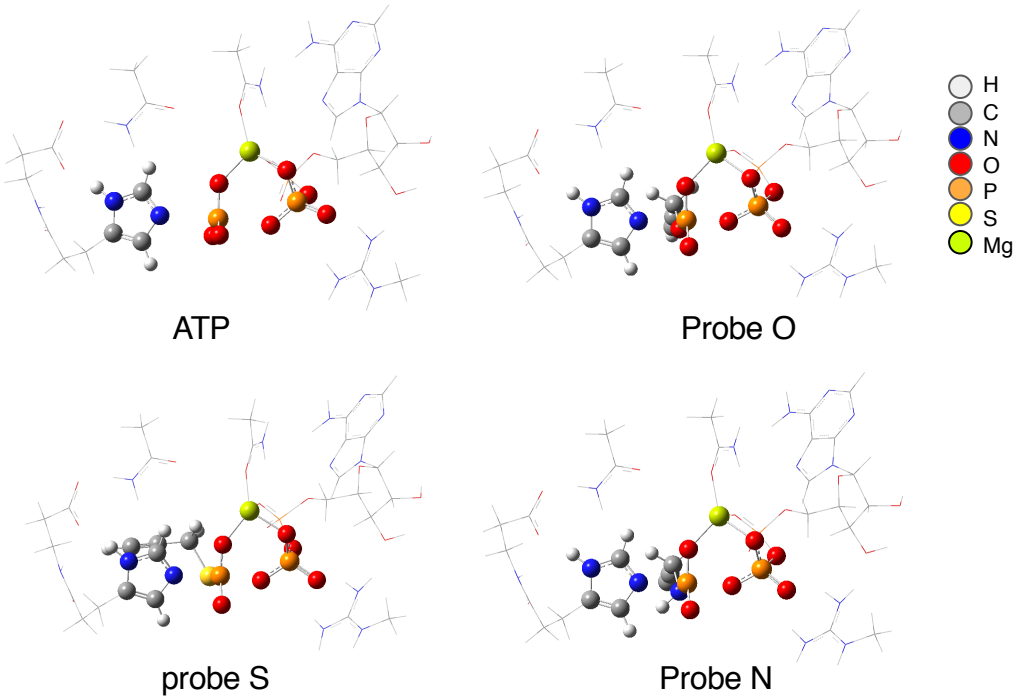

Supplementary Figure 16. Comparison of the transition state (TS1) structures of the phosphohistidine formation for ATP and Probes O, S and N.

Computational details for calculating p*K*a(s):

The pK_a can be calculated from the Gibbs free energy of the acid dissociation reaction in solution:[6]

$$pK_a = \Delta G_{aq}/2.303RT \qquad (1)$$

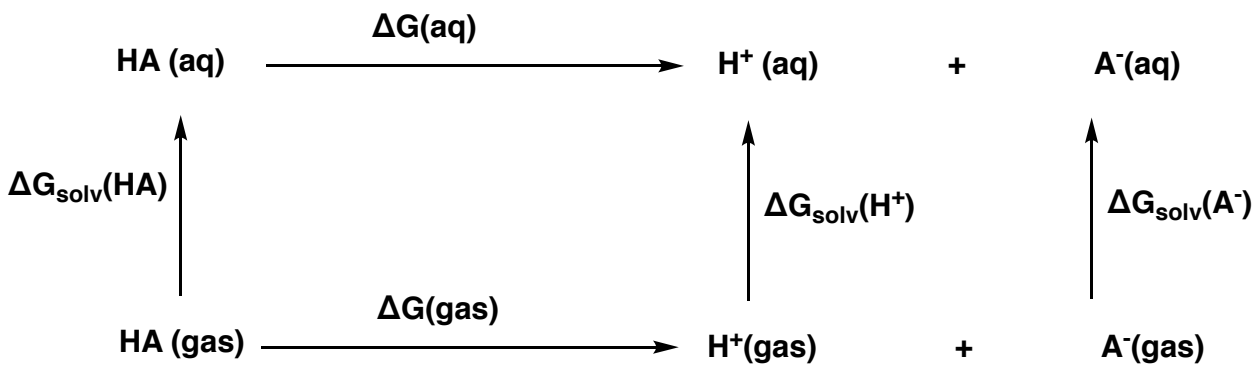

Supplementary Figure 17. Thermodynamic cycle of acid dissociation.

ΔG_{aq} can be obtained from the thermodynamic cycle in **Supplementary Figure 17** using the following equation:

$$\Delta G_{aq} = \Delta G_{gas} + \Delta\Delta G_{solv} = \Delta E_{gas} + \Delta G^{corr} + \Delta\Delta G_{solv} \quad (2)$$

with

$$\Delta G_{gas} = G_{gas}(H^+) + G_{gas}(A^-) - G_{gas}(HA) \qquad (3)$$

$$\Delta\Delta G_{solv} = \Delta G_{solv}(H^+) + \Delta G_{solv}(A^-) - \Delta G_{solv}(HA) \qquad (4)$$

where ΔG_{gas} and ΔG_{aq} denotes the Gibbs free energy change of acid dissociation reaction in gas phase and solution phase, $\Delta\Delta G_{solv}$ denotes the solvation free energy change. The free energy in gas phase is conventionally summed up by the electronic energy ΔE_{gas} computed at high level, and the thermal correction to Gibbs free energy computed at low level in gas phase. When gas-phase and solution-phase geometries are similar, using gas-phase geometries for calculations in eq. (1) is a convention and an accurate approximation. However, for species given in **Supplementary Figure 18** and **Supplementary Figure 19**, the gas-phase and solution-phase geometries are sometimes significantly different. Under such circumstances, using solution-phase geometries and vibrational corrections is more appropriate.[7] Therefore, we calculated every term in eq. (2) based on the geometries optimized with three DFT: B3LYP-D3, M06-2X[8] and ωB97XD[9], with 6-311+G(d,p) basis set and SMD implicit solvent model, and obtain the ΔG^{corr} at the same level of method used for geometry optimization. E_{gas} was computed with B2PLYPD3/ma-TZVP in gas phase,[10-11] where ma-TZVP basis set is the "minimally augmented" def2-TZVP basis set with s and p diffuse basis functions on non-hydrogenic

atoms. ΔG_{solv} was taken from the difference of electronic energy with M05-2X[12]/6-31+G(d) and M05-2X/6-31+G(d)/SMD(water) as suggested by Marenich et al.[13]

Most of systems of interest are charged systems and have rather different geometry in gas phase and solution phase, we also used the direct approach recommended by Ho.[14] He suggested to calculate ΔG_{aq} directly within the SMD solvation model for systems where solvation induced changes in geometry are significant:

$$\Delta G_{aq}(\mathbf{R_l}) = \Delta E^{H}_{aq}(\mathbf{R_l}) + \Delta G^{corr,L}_{aq}(\mathbf{R_l}) \qquad (5)$$

where $\mathbf{R_l}$ denotes solution-phase geometry, E^{H}_{aq} is the solution-phase electronic energy at high level, and $G^{corr,L}_{aq}$ is the thermal corrections to Gibbs free energy computed in solution-phase at low level. In our calculations, the geometry optimization and thermal correction to Gibbs free energy are obtained using 6-311+G(d,p) basis set and SMD solvent model with three DFT: B3LYP-D3, M06-2X and ωB97XD; E^{H}_{aq} is obtained using B2PLYPD3/ma-TZVP/SMD.

Using $G_{gas}(H^+)$ = -6.28 kcal.mol^{-1}, $\Delta G_{solv}(H^+)$ = -265.9 kcal.mol^{-1}, and 1.89 kcal.mol^{-1} for conversion between 1 atm to 1 M at 298.15 K,[13] we get the final expression of pK_a:

$$pK_a = 0.733 \times [\, G_{gas}(A^-) - G_{gas}(AH) + \Delta G_{solv}(A^-) - \Delta G_{solv}(AH) - 270.29 \,] \quad (6)$$

We first calculated the absolute pK_as using eq (6).

Supplementary Table 3. Calculated absolute pKa values with thermodynamic cycles. pKa1/ pKa2/ (pKa3) are given for phosphate (and its derivatives) and phosphohistidine (and its derivatives). Electronic energies are calculated using B2PLYPD3/ma-TZVP. The solvation energies are calculated by the difference between M05-2X/6-31+G(d)/SMD and M05-2X/6-31+G(d).

Species	Geometry optimization and thermal correction method		
	B3LYP-D3	M06-2X	ωB97XD
Phosphate	-0.2 / 10.4 / 18.2	0.1 / 10.5 / 17.9	-0.2 / 10.3 / 17.9
Propargyl phosphate	-1.8 / 9.6	-1.5 / 9.6	-1.9 / 9.7
Propargyl thiophosphate	-3.2 / 8.7	-2.8 / 8.6	-3.2 / 8.5
Phosphohistidine	-18.0 / -9.2 / 3.9	-19.1 / -8.3 / 3.8	-17.9 / -9.3 / 3.8
Propargyl phosphohistidine	-19.7 / -8.0	-19.9 / -8.2	-19.3 / -8.4
Propargyl thiophosphohistidine	-20.9 / -11.1	-20.3 / -11.0	-22.1 / -9.9

Supplementary Table 4. Calculated absolute pKa values with direct approach pKa1/ pKa2/ (pKa3) are given for phosphate (and its derivatives) and phosphohistidine (and its derivatives). Electronic energies are calculated using B2PLYPD3/ma-TZVP/SMD.

Species	Geometry optimization and thermal correction method		
	B3LYP-D3	M06-2X	ωB97XD
Phosphate	0.5 /11.8 / 23.1	0.8 / 12.0 / 22.8	0.5 / 11.8 / 22.8
Propargyl phosphate	-0.8 / 11.1	-0.5 / 11.1	-0.9 / 11.3
Propargyl thiophosphate	-2.5 / 9.9	-2.1 / 9.8	-2.5 / 9.8
phosphohistidine	-17.7 / -8.5 / 5.4	-18.8 / -7.3 / 5.3	-17.6 / -8.5 / 5.3
Propargyl phosphohistidine	-19.2 / -6.8	-19.3 / -7.1	-18.8 / -7.3
Propargyl thiophosphohistidine	-20.4 / -9.8	-19.7 / -9.7	-21.6 / -8.6

By comparing the results in **Supplementary Table 3** and **Supplementary Table 4** to the experimental p*K*a values of phosphoric acid (H_3PO_4, pK_{a1}=2.16, pK_{a2}=7.21, and pK_{a3}=12.32),[17] we found that there were large errors in calculating absolute p*K*a values. This is not surprising since we applied an implicit solvent model to charged systems.[13] Although we can improve the accuracy of our results by including several explicit water molecules, the intrinsic difficulty in modeling charged species via dielectric continuum model is inevitable. Additionally, the effect and protonation state of the amino acid side chain attached to histidine is complex and unclear. Therefore, to minimize the errors for calculated p*K*a values, we also calculated relative p*K*a values and scaled p*K*a values.

Relative p*K*a values are calculated using eq. (7), and the experimental pK_{a1}, pK_{a2}, and pK_{a3} of H_3PO_4 are used as references. Depending on the charge of acid AH, the reference acid BH is chosen among H_3PO_4, $H_2PO_4^-$, or HPO_4^{2-} to minimize the charge difference between AH and BH, and therefore achieves maximum error cancellation.

$$pK_{a\,(calc,\,AH)} = 0.733 \times [\,\Delta G_{aq}\,(calc,\,AH) - \Delta G_{aq}\,(calc,\,BH)\,] + pK_{a\,(ref,\,BH)} \quad (7)$$

Scaled p*K*a values are calculated by plugging the absolute p*K*a values of species without experimental values into the linear regression of absolute and experimental p*K*a values of H_3PO_4. The coefficient of determination (R^2) is larger than 0.999 for direct approach, and larger than 0.989 for thermodynamic cycle. Since relative and scaled p*K*a values calculated using thermodynamic cycle and direct approach are similar (within 0.5 p*K*a) in most cases, we only showed the results of thermodynamic cycle in **Supplementary Figures 18** and **19**.

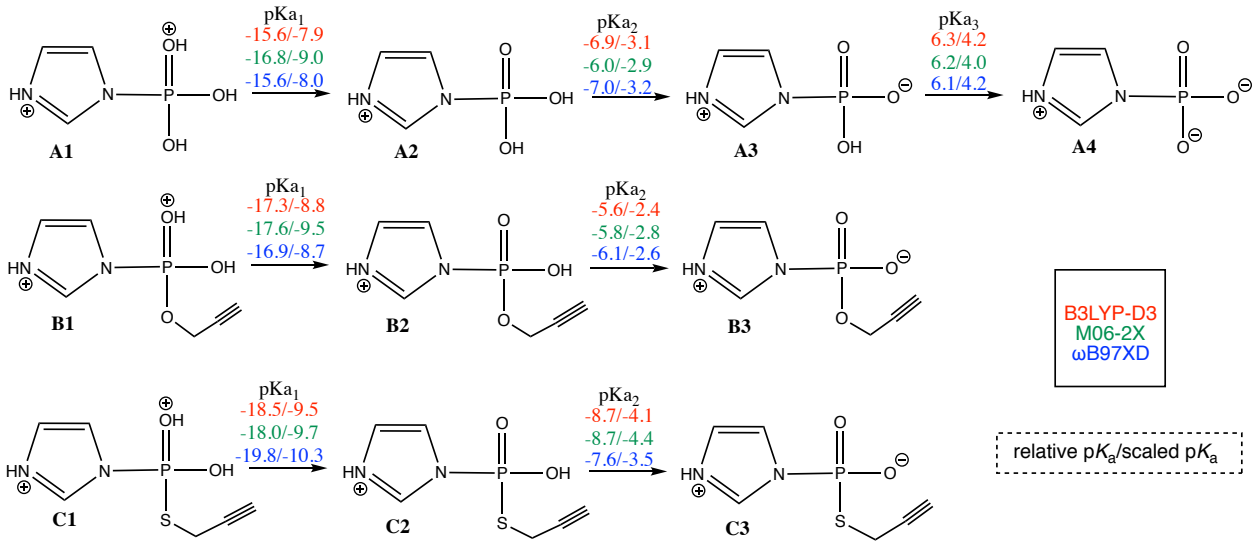

Supplementary Figure 18. Calculated p*K*a values for phosphohistidine and its derivatives.

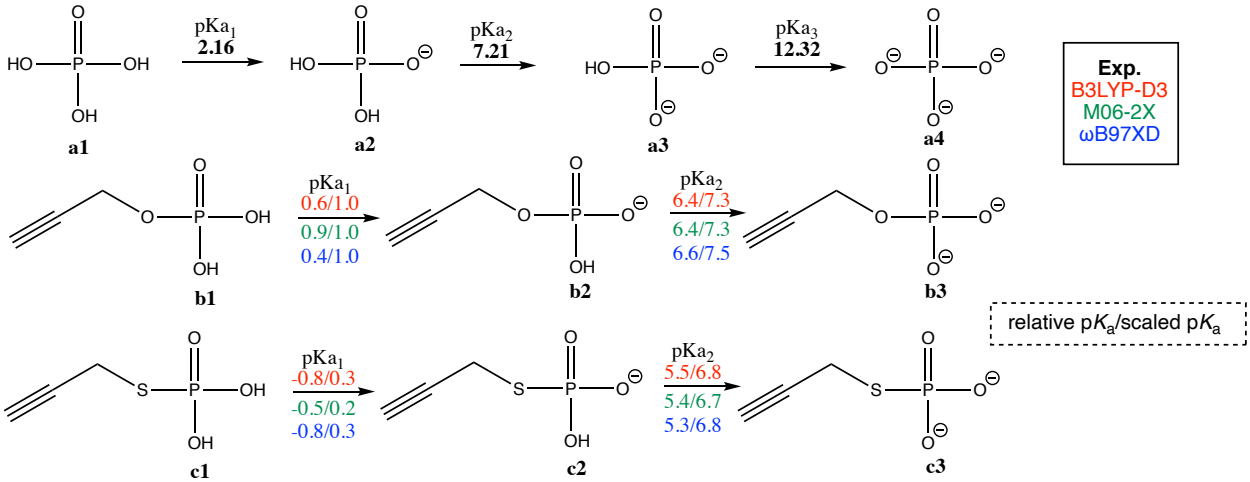

Supplementary Figure 19. Experimental p*K*a values for phosphate and calculated p*K*a values for its derivatives.

In **Figure Supplementary Figure 18**, we simplified the computational model by using imidazole instead of histidine, or H243+D244 residues as we used previously in the phosphohistidine formation. We calculated the p*K*a values using imidazole and using H243+D244 at low level, the difference is less than 0.5 pK_a at most cases. When the imidazole nitrogen is protonated, the weak P-N bond in phosphohistidine is susceptible to hydrolysis. Therefore, we assume the imidazole nitrogen that does not bind to phosphate is always protonated at the experimentally tested pH 1-7.

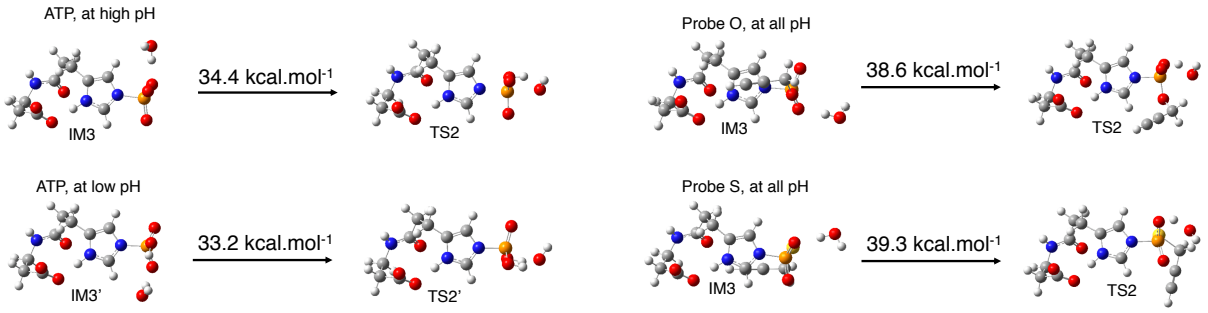

Supplementary Figure 20. Calculated reaction barriers for phosphohistidine hydrolysis with single water (1W) path. The geometry optimization and Gibbs free energies are calculated using B3LYP-D3/6-31+G(d)/SMD.

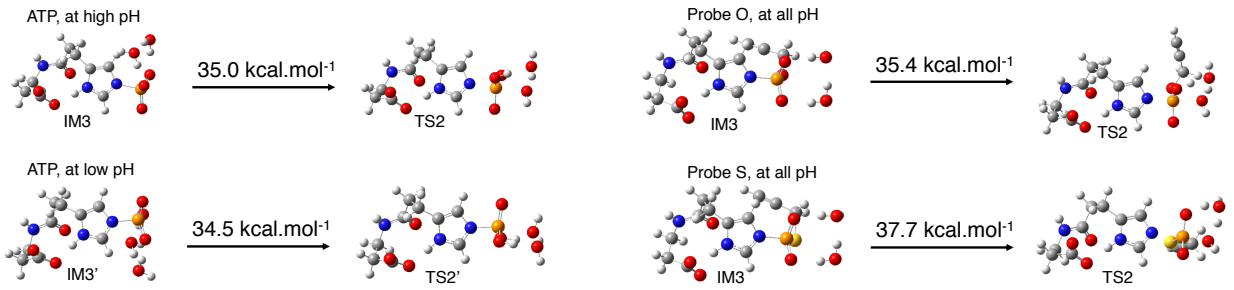

Supplementary Figure 21. Calculated reaction barriers for phosphohistidine hydrolysis with two water (2W) path. The geometry optimization and Gibbs free energies are calculated using B3LYP-D3/6-31+G(d)/SMD.

We calculated the reaction barriers based on the single water (1W) mechanism and two water (2W) mechanism proposed by Prasad et al.[15] The results are presented in **Supplementary Figures 20** and **21**. Based on the results in **Supplementary Figure 19**, the phosphorylated imidazole resulting from the phosphorylation of imidazole with ATP is protonated at pH = 4.0-6.3, while the reactants resulting from phosphorylation with **Probes O** and **S** are always fully protonated. The higher formation barriers for the phosphorylated products resulting from **Probes O** and **S** and compared to the one resulting from ATP indicate that their phosphohistidine species should be more stable. The 1W and 2W mechanism give similar results, while 2W mechanism suggests **Probe O** and ATP have similar reaction barrier. The 2W mechanism agrees with experimental results well. However, the hydrolysis process slows down for the phosphorylated species resulting from **Probes O** and **S** while speeds up for the one coming from ATP at pH = 1. Therefore, we studied the reaction thermodynamics to understand this phenomenon.

To obtain accurate reaction thermodynamics, we calculated the high-level electronic energy using ma-TZVP basis with three different methods: M06-2X, B2PLYPD3, and DLPNO-CCSD(T). DLPNO-CCSD(T) calculations were performed in ORCA electronic structure package.[16] With the knowledge of calculated p*K*a values, we were able to show how reaction thermodynamics change with respect to decreasing pH in **Supplementary Figures 22 to 24**.

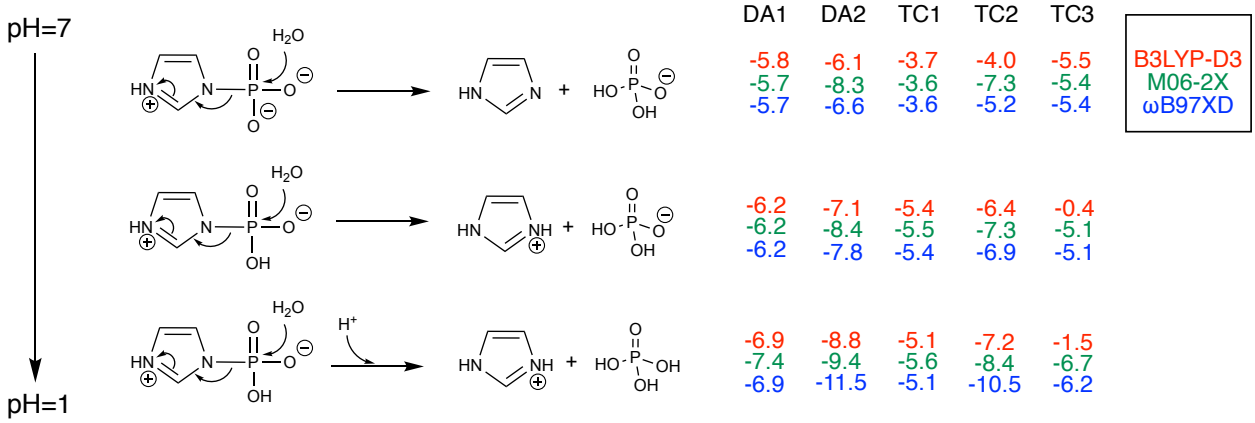

Supplementary Figure 22. Calculated reaction thermodynamics (kcal.mol^{-1}) for the hydrolysis of phosphorylated imidazole at pH = 1 to 7. The experimental free energy -270.29 kcal.mol^{-1} is used for the proton. Geometries and thermal corrections were obtained at 6-311+G(d,p) basis and SMD with three DFT: B3LYP-D3 (red), M06-2X (green) and ωB97XD (blue). Reaction thermodynamics were calculated using 5 different methods. **DA**: direct approach; **TC**: thermodynamic cycle. **DA1**: electronic energies were calculated by B2PLYPD3/ma-TZVP/SMD; **DA2**: electronic energies were calculated by the same DFT used for geometry optimization with ma-TZVP and SMD; **TC1**: electronic energies were calculated using B2PLYPD3/ma-TZVP in gas phase; **TC2**: electronic energies were calculated by the same DFT used for geometry optimization with ma-TZVP in gas phase; **TC3**: electronic energies were calculated by DLPNO-CCSD(T)/ma-TZVP in gas phase.

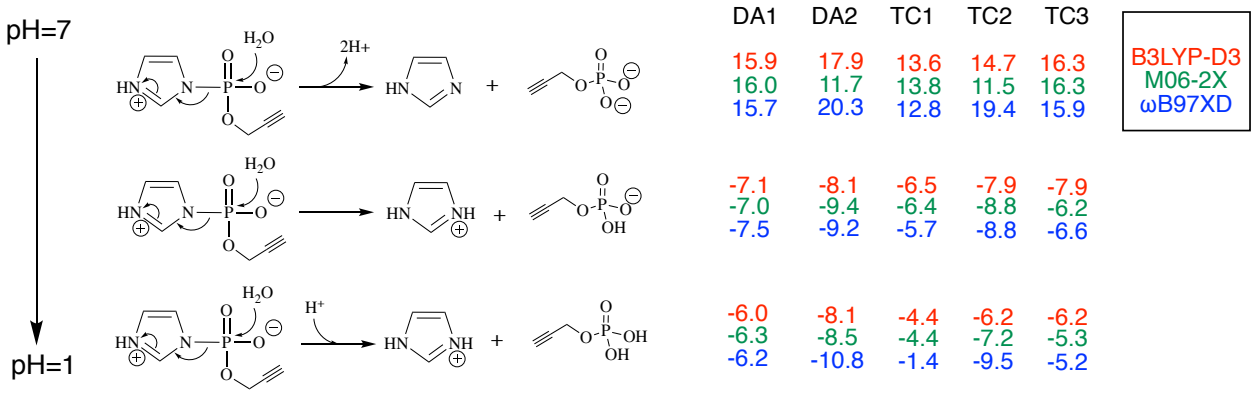

Supplementary Figure 23. Calculated reaction thermodynamics (kcal.mol^{-1}) for the hydrolysis of the propargyl phosphoimidazole at pH = 1 to 7. Geometries and thermal corrections were obtained at 6-311+G(d,p) basis and SMD with three DFT: B3LYP-D3 (red), M06-2X (green) and ωB97XD (blue).

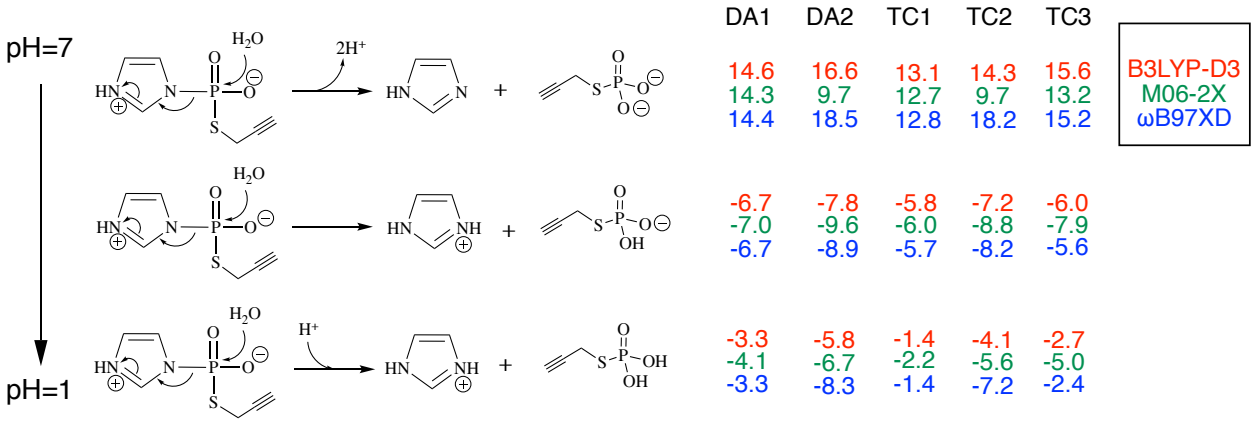

Supplementary Figure 24. Calculated reaction thermodynamics (kcal.mol^{-1}) for the hydrolysis of the propargyl thiophosphoimidazole at pH = 1 to 7. Geometries and thermal corrections are obtained at 6-311+G(d,p) basis and SMD with three DFT: B3LYP-D3 (red), M06-2X (green) and ωB97XD (blue).

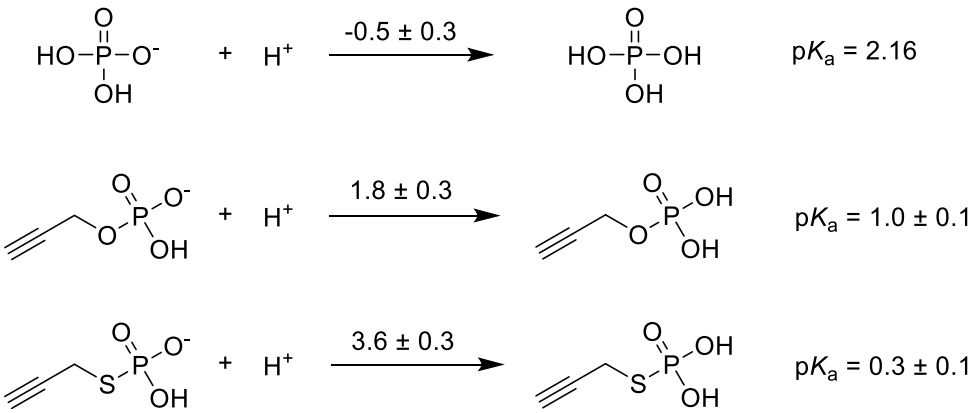

Supplementary Figure 25. Calculated reaction thermodynamics (kcal.mol^{-1}, given above arrow) for protonation of inorganic phosphate, propargyl phosphate, and propargyl thiophosphate at pH 1. The reaction thermodynamics and pK_a values were calculated by taking the average and standard error of double-hydride DFT calculations and DLPNO-CCSD(T) correspond to dataset TC1 and TC3 in **Supplementary Figures 22 to 24,** except the pK_a of phosphate, which has been determined experimentally.[17]

We found that the pH critically affects the reaction thermodynamics by changing the protonation state of hydrolysis products. The different protonation states for hydrolysis reactants and products are labeled in **Supplementary Figures 18** and **19**. For ATP, lowering the pH always decreases the reaction thermodynamics. At around pH = 5, the reactant changes from A4 to A3, and the reaction barrier changes from 35.1 kcal.mol^{-1} to 33.2 kcal.mol^{-1} in the 1W mechanism, and from 35.0 kcal.mol^{-1} to 34.5 kcal.mol^{-1} in 2W mechanism. At pH = 2.1, the product changes from **a2** to **a1**, and the reaction thermodynamics decrease.

Interestingly, for **Probe O** and **Probe S,** the reaction thermodynamics initially decrease, but then, increase again at low pH. For **Probe O**, at around pH = 6, the product changes from **b3** to **b2** and the reaction thermodynamics decrease (**Supplementary Figure 23**). However, at around pH = 1, the product changes from **b2** to **b1**, and the reaction thermodynamics increase. For **Probe S**, at around pH = 4, the product changes from **c3** to **c2**, and the reaction thermodynamics decrease. At around pH = -1, the product changes from **c2** to **c1**, and the reaction thermodynamics increase.

Due to the limitation of applying implicit solvent model to charged systems and using experimental free energy of proton in calculations, we have difficulty in obtaining strong quantitative agreement between theory and experiment for the p*K*a values and thermodynamic data. Therefore, since at a given pH, there should be an equilibrium mixture of protonation states and our p*K*a values likely have some quantitative error, we report the larger number of protons expected for a pH. Specifically, we have reported the reaction thermodynamics for pH = 7, pH = 5-3, and pH = 1 to be the b3, b2, and b1 products for **Probe O**. We have reported the reaction thermodynamics for pH = 7, pH = 5–3, and pH = 1 to be the c3, c2, and c1 products for **Probe S**. While there may be some quantitative uncertainty of our calculations, there is a clear qualitative agreement between

the experimental and computational results. We attribute the pH-dependent stability of phosphorylated HK853 to the relative stability of the phosphohistidine and phosphate hydrolysis products at different protonation states.

REFERENCES

1. Wilke, K. E.; Francis, S.; Carlson, E. E. (2012) Activity-Based Probe for Histidine Kinase Signaling. *J. Am. Chem. Soc. 134*, 9150–9153.
2. Chan, T. R.; Hilgraf, R.; Sharpless, K. B.; Fokin, V. V. (2004) Polytriazoles as Copper(I)-Stabilizing Ligands in Catalysis. *Org. Lett. 6*, 2853–2855.
3. Chase, O. M.; Espinasse, A.; Wilke, K. E.; Carlson, E. E. (2018) Exploration of the Effects of γ-Phosphate-Modified ATP Analogues on Histidine Kinase Autophosphorylation. *Biochemistry 57*, 4368–4373.
4. Ueno, T. B.; Johnson, R. A.; Boon, E. M. (2015) Optimized assay for the quantification of histidine kinase autophosphorylation. *Biochem. Biophys. Res. Commun. 465* (3), 331–337.
5. Frisch, M. J.; Trucks, G. W.; Schlegel, H. B.; Scuseria, G. E.; Robb, M. A.; Cheeseman, J. R.; Scalmani, G.; Barone, V.; Petersson, G. A.; Nakatsuji, H.; Li, X.; Caricato, M.; Marenich, A. V.; Bloino, J.; Janesko, B. G.; Gomperts, R.; Mennucci, B.; Hratchian, H. P.; Ortiz, J. V.; Izmaylov, A. F.; Sonnenberg, J. L.; Williams; Ding, F.; Lipparini, F.; Egidi, F.; Goings, J.; Peng, B.; Petrone, A.; Henderson, T.; Ranasinghe, D.; Zakrzewski, V. G.; Gao, J.; Rega, N.; Zheng, G.; Liang, W.; Hada, M.; Ehara, M.; Toyota, K.; Fukuda, R.; Hasegawa, J.; Ishida, M.; Nakajima, T.; Honda, Y.; Kitao, O.; Nakai, H.; Vreven, T.; Throssell, K.; Montgomery Jr., J. A.; Peralta, J. E.; Ogliaro, F.; Bearpark, M. J.; Heyd, J. J.; Brothers, E. N.; Kudin, K. N.; Staroverov, V. N.; Keith, T. A.; Kobayashi, R.; Normand, J.; Raghavachari, K.; Rendell, A. P.; Burant, J. C.; Iyengar, S. S.; Tomasi, J.; Cossi, M.; Millam, J. M.; Klene, M.; Adamo, C.; Cammi, R.; Ochterski, J. W.; Martin, R. L.; Morokuma, K.; Farkas, O.; Foresman, J. B.; Fox, D. J. (2016) *Gaussian 16 Rev. C.01*, Wallingford, CT.
6. Liptak, M. D.; Gross, K. C.; Seybold, P. G.; Feldgus, S.; Shields, G. C. (2002) Absolute pKa Determinations for Substituted Phenols. *J. Am. Chem. Soc. 124*, 6421–6427.
7. Ribeiro, R. F.; Marenich, A. V.; Cramer, C. J.; Truhlar, D. G. (2011) Use of Solution-Phase Vibrational Frequencies in Continuum Models for the Free Energy of Solvation. *J. Phys. Chem. B 115*, 14556–14562.
8. Zhao, Y.; Truhlar, D. G. (2008) Density Functionals with Broad Applicability in Chemistry. *Acc. Chem. Res. 41*, 157–167.
9. Chai, J.-D.; Head-Gordon, M. (2008) Long-range corrected hybrid density functionals with damped atom–atom dispersion corrections. *Phys. Chem. Chem. Phys. 10*, 6615–6615.
10. Weigend, F.; Ahlrichs, R. (2005) Balanced basis sets of split valence, triple zeta valence and quadruple zeta valence quality for H to Rn: Design and assessment of accuracy. *Phys. Chem. Chem. Phys. 7*, 3297–3297.
11. Zheng, J.; Xu, X.; Truhlar, D. G. (2011) Minimally augmented Karlsruhe basis sets. *Theor. Chem. Acc. 128*, 295–305.
12. Yan, Z.; Schultz, N. E.; Truhlar, D. G. (2006) Design of Density Functionals by Combining the Method of Constraint Satisfaction with Parametrization for Thermochemistry, Thermochemical Kinetics, and Noncovalent Interactions. *J Chem Theory Comput. 2*, 364–382.
13. Marenich, A. V.; Cramer, C. J.; Truhlar, D. G. (2009) Universal Solvation Model Based on Solute Electron Density and on a Continuum Model of the Solvent Defined by

the Bulk Dielectric Constant and Atomic Surface Tensions. *J. Phys. Chem. B 113*, 6378–6396.
14. Ho, J. (2015) Are thermodynamic cycles necessary for continuum solvent calculation of pKas and reduction potentials? *Phys. Chem. Chem.Phys. 17*, 2859–2868.
15. Prasad, B. R.; Plotnikov, N. V.; Warshel, A. (2013) Addressing Open Questions about Phosphate Hydrolysis Pathways by Careful Free Energy Mapping. *J. Phys. Chem. B 117*, 153–163.
16. Neese, F. (2018) Software update: the ORCA program system, version 4.0. *Wiley Interdisciplinary Reviews: Computational Molecular Science 8*, e1327–e1327.
17. Lide, D. R. (2004) CRC Handbook of Chemistry and Physics. *J. Am. Chem. Soc. 126*, 1586–1586.